Optical Materials xxx (2016) xxx–xxx

Contents lists available at ScienceDirect

Optical Materials

journal homepage: www.elsevier.com/locate/optmat

Rare earth doped glass–ceramics containing $NaLaF_4$ nanocrystals

E. Elsts *, G. Krieke, U. Rogulis, K. Smits, A. Zolotarjovs, J. Jansons, A. Sarakovskis, K. Kundzins

Institute of Solid State Physics, University of Latvia, 8 Kengaraga Street, Lv-1063 Riga, Latvia

ARTICLE INFO

Article history:
Received 23 October 2015
Received in revised form 5 January 2016
Accepted 5 January 2016
Available online xxxx

Keywords:
Glass
Glass–ceramics
Cathodoluminescence
X-ray induced luminescence
XRD
SEM
Decay times

ABSTRACT

Oxyfluoride glasses $16Na_2O–9NaF–5LaF_3–7Al_2O_3–63SiO_2$ (mol%) activated with 3% terbium, dysprosium, praseodymium and neodymium fluorides have been prepared and studied by differential thermal analysis, cathodoluminescence, X-ray induced luminescence, X-ray diffraction, scanning electron microscopy and energy dispersive X-ray spectroscopy. We found out that the presence of crystalline phase enhances the X-ray induced luminescence intensity. X-ray induced luminescence is the most intense for the sample activated with terbium and treated at 700 °C, whereas the praseodymium and neodymium activated samples have the fastest decay times.

1. Introduction

Rare earth activated glasses and glass–ceramics can be used as scintillators for high-energy physics, X-ray computed tomography and radiation monitoring [1]. Ceramic and glass scintillators can be made in various shapes and sizes if correctly cooled after glass casting. Cost advantages over single crystals appear when large detectors are necessary. Rare earth ceramic materials have potential application as X-ray scintillator for slow event detection [2] in tomography [3] for medicine and geology.

Slow scintillators are sometimes preferable because the large difference of scintillation decay times makes it easy to process the signal in such applications as phoswich ("phosphor sandwich") detectors, where two different scintillation materials are used. For example, BGO (300 ns) and Ce-doped GSO (60 ns) are used in actual detectors. Sometimes, very fast (20–30 ns) and fast (100 ns) scintillators are coupled [4].

Oxyfluorides materials combine low phonon energy of the fluoride crystals and a transparency, mechanical and chemical resistance of the aluminosilicate glasses [5].

Materials with lower phonon energy are good luminescent hosts because they suppress the non-radiative loss and to obtain higher quantum efficiency [6].

Phonon energy of $NaLaF_4$ (280 cm^{-1}) is significantly lower than phonon energy of phosphate (1200 cm^{-1}) and silicate (1100 cm^{-1}) glasses [5–7].

$NaLaF_4$ have been synthesized as polycrystalline powder by solid state reaction [8], as single crystals by Czochralski method [9], by sol–gel method [10] and as crystals embedded in the glass–ceramic by melting [11]. $NaLaF_4$ glass–ceramics containing RE ions (Tm^{3+}, Eu^{3+}, Yb^{3+}, Er^{3+}) were synthesized and studied [12].

In this research we have synthesized new $NaLaF_4$ containing glass and glass–ceramic samples activated with Tb^{3+}, Dy^{3+}, Pr^{3+} and Nd^{3+}. We have analyzed their structure and luminescence properties.

2. Experimental

Glass samples with nominal composition $16Na_2O–9NaF–5LaF_3–7Al_2O_3–63SiO_2$ (mol%) doped with 3 mol% of one of the following rare earth activator components: TbF_3, DyF_3, PrF_3 and NdF_3, were prepared by melting the appropriate batch materials (Na_2CO_3, NaF, LaF_3, Al_2O_3, SiO_2, TbF_3, PrF_3, NdF_3 and DyF_3).

The samples hereinafter will be referred as NLF (non doped), NLF:Tb, NLF:Dy, NLF:Pr and NLF:Nd.

The batches of 10 g were melted in covered corundum crucibles at ambient atmosphere at 1500 °C for 30 min. The melts were casted in stainless steel molds.

NLF:Tb and NLF:Dy samples are colorless, NLF:Pr are green–yellow and NLF:Nd – violet–purple.

* Corresponding author.
E-mail address: eelsts@cfi.lu.lv (E. Elsts).

http://dx.doi.org/10.1016/j.optmat.2016.01.005
0925-3467/

The temperatures for this heat treatment were estimated from differential thermal analysis (DTA). It was made on powdered sample with a 10 °C/min heating rate using BÄHR-Thermoanalyse GmbH Differential Thermal Analyzer DTA/DSC 703 and Al_2O_3 reference.

Glass samples were converted to glass–ceramics by thermal treatment at 600 °C, 700 °C and 800 °C temperature for 30 min. Temperature ramp rate was 10 °C/min. After heat treatment samples lose their transparency.

The formation of crystalline phases in samples has been investigated by the X-ray diffractometer X'Pert PRO with the Cu tube at 40 kV and 30 mA, the PDF-2 database was used.

The X-ray excited luminescence spectra were recorded by Andor Shamrock B303-I spectrograph equipped with a CCD camera (Andor DU- 401A-BV). The surfaces of all samples were of equal size. X-ray irradiation parameters were the following: W anode, 30 kV, 10 mA.

Cathodoluminescence (CL) spectra and decay curves have been registered by a bialkaline photocathode photomultiplier ΦΕΥ-106 with spectral range 180–830 nm and counting board M9003 Hamamatsu with a special program.

Pulsed beam of 6 kV electrons was used for cathodoluminescence experiments. For studies of decay times, a method of many strobes has been used.

SEM-FIB Tescan Lyra and EDX Oxford X-Max with 50 mm^2 detector, AZtec software has been used for SEM (scanning electron microscopy) and EDS (energy dispersive X-ray spectroscopy) analysis.

3. Results and discussion

3.1. Sample characterization by DTA

Fig. 1 shows DTA of NLF:Tb glass sample. Endothermic peak indicates the glass transition temperature which is located at about 480 °C. Exothermic peak starting at 670 °C shows crystallization temperature. The most intense heat release and therefore the most intense crystallization have been reached at 725 °C. Thermal treatment temperatures were chosen between the above mentioned peaks.

3.2. Sample characterization by XRD

X-ray diffraction patterns were similar irrespective of the dopant. Intense peaks of the $NaLaF_4$ nanocrystals (shown by circles) have been observed for the samples, which were heat treated at 600 °C and 700 °C. For some samples the less intense peaks of the LaOF nanocrystals (Fig. 2) have been observed. The formation of LaF_3, britholite $(LaTb)_5(SiO_4)_3(O,F)$ and nepheline $(NaAlSiO_4)$ nanocrystals have been observed for the samples, which were heat treated at 800 °C. Britholite and nepheline correspond to the lower peaks located between 20° and 33° in the XRD pattern. $NaLaF_4$ decomposition temperature is 786 °C [13]. However, $NaLaF_4$ nanocrystals still exist after heat treatment at 800 °C.

Size of nanocrystals D was estimated using Scherrer's equation:

$$D = \frac{K\lambda}{\beta \cos\theta}. \quad (1)$$

Although the symmetry of $NaLaF_4$ crystal is hexagonal [14], nanocrystals do not grow hexagonal, but mostly remain spherical. Scherrer constant K has been taken 0.89 for a spherical crystallite [15]. λ (nm) represents the wavelength of Cu Kα radiation. θ is the Bragg angle of the XRD peak and β – line broadening at half of the maximum intensity (FWHM) of the XRD peak. Bragg angle and FWHM were determined using PANalytical X'Pert Data Viewer. Results show the dependence of nanocrystal size on the heat treatment temperature (Table 1).

From the obtained results we can summarize that the larger nanocrystals are formed in the samples subjected to the higher temperature heat treatment. This trend is applicable to heat treatment up to 800 °C.

3.3. Sample characterization by SEM

SEM–EDX images show approximately 500 nm large areas with a higher concentration of the sodium, lanthanum, fluorine and rare earth activator (Fig. 3). Size of this area exceeds crystallite size, which could be calculated by Scherrer equation.

Therefore, several nanocrystals could be located in these areas. Rare earth ions could be incorporated in the $NaLaF_4$ matrix.

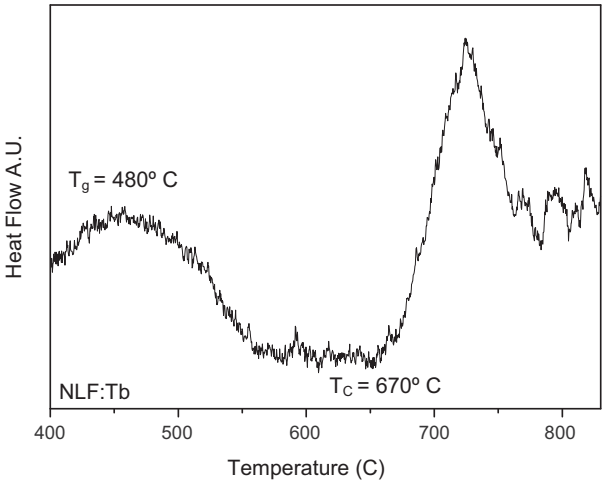

Fig. 1. DTA curve of NLF:Tb glass sample.

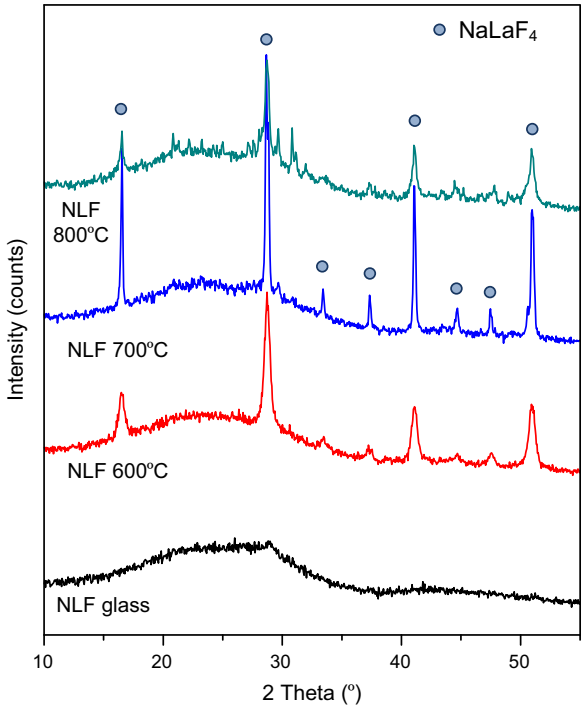

Fig. 2. X-ray diffraction pattern of NLF (non-doped) samples. Peaks belonging to $NaLaF_4$ nanocrystals are shown by circles.

Table 1
Mean size of crystallites in the samples after different heat treatments. Uncertainty is approximately ±10%.

Sample	Heat treatment		
	600 °C	700 °C	800 °C
	Crystallite size (nm)		
NLF:Tb	32	39	45
NLF:Dy	32	36	38
NLF:Pr	34	44	47
NLF:Nd	32	39	37
NLF (non doped)	19	45	53

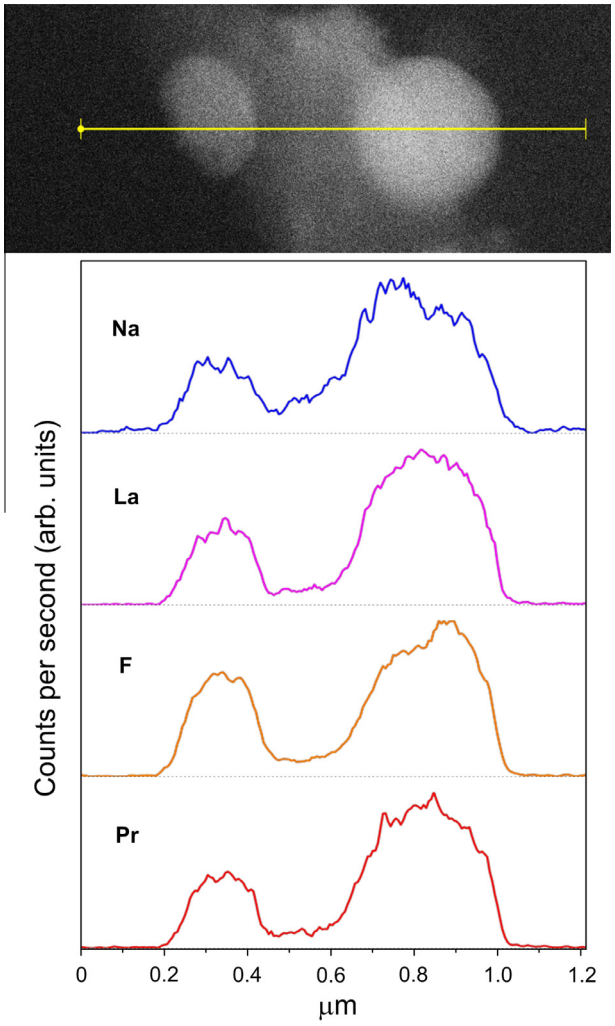

Fig. 3. SEM EDX images of the NLF:Pr 800 °C sample.

3.4. Luminescent properties

X-ray induced luminescence spectra for glass and the samples heat treated at 600 °C, 700 °C, 800 °C as well as cathodoluminescence spectra and decay times for the samples heat treated at 700 °C have been measured.

Luminescence of all studied rare earth ($Tb^{3+}(4f^8)$, $Dy^{3+}(4f^9)$, $Pr^{3+}(4f^2)$, $Nd^{3+}(4f^3)$) activated samples is caused by the corresponding f–f transitions. Tb^{3+}, Dy^{3+} have stronger emission than Pr^{3+}, Nd^{3+} [16].

The electron levels for transitions of the corresponding luminescence bands were determined using data from the articles [17–23].

However, the wavelength position of the most intense peaks may differ in the cathodoluminescence and X-ray induced spectra. We must also take into account that cathodoluminescence spectrometer could not measure spectra in the infrared range.

3.4.1. X-ray induced luminescence of NLF:Tb

The X-ray induced luminescence spectra (Fig. 4) of NLF:Tb samples show peaks at approximately 379 nm, 418 nm, 436 nm, 458 nm, 489 nm, 541 nm, 589 nm and 626 nm corresponding to the energy levels transitions $^5D_3 \rightarrow {}^7F_J$ ($J = 6, 5, 4, 3$) and $^5D_4 \rightarrow {}^7F_J$ ($J = 6, 5, 4, 3$). The most intense peaks are located at approximately 545 nm and correspond to $^5D_4 \rightarrow {}^7F_5$ transition.

In the X-ray induced luminescence spectra intensity of peaks belonging to the "green" group $^5D_3 \rightarrow {}^7F_J$ ($J = 6, 5, 4, 3$) is significantly higher than intensity of the "blue" group $^5D_4 \rightarrow {}^7F_J$ ($J = 6, 5, 4, 3$), which is shown magnified. The blue group is suppressed due to the known cross relaxation effect at high Tb^{3+} doping level.

Shapes of the curves of different heat treated samples are similar, but the integrated intensities vary. The sample NLF:Tb 700 °C emits the most intense integrated luminescence.

Since in the XRD pattern of NLF:Tb 700 °C dominate peaks $NaLaF_4$ nanocrystals, we suppose that the enhanced luminescence of the NLF:Tb 700 °C could be explained by embedding of the Tb^{3+} in $NaLaF_4$ nanocrystals.

3.4.2. X-ray induced luminescence of NLF:Dy

X-ray induced luminescence spectra (Fig. 5) of NLF:Dy samples show peaks at 483 nm, 574 nm, 667 nm, 756 nm and 843 nm corresponding to energy levels transitions $^4F_{9/2} \rightarrow {}^6H_{15/2}$, $^6H_{13/2}$, $^6H_{11/2}$, $^6H_{9/2}$, $^6H_{7/2}$. The maximal peak belongs to the transition $^4F_{9/2} \rightarrow {}^6H_{13/2}$ and is located at 574 nm. The most intense X-ray induced luminescence is emitted by the heat treated at 800 °C NLF:Dy sample. We could assume that dysprosium incorporates in further crystalline phases, which appear at 800 °C.

3.4.3. X-ray induced luminescence of NLF:Pr

The X-ray induced luminescence spectra of NLF:Pr samples (Fig. 6) show energy transitions form $^1S_0$ and $^3P_0$ energy levels. $^1S_0 \rightarrow {}^3F_{3,4}$, $^1G_4$, $^1D_2$, $^1I_6$ energy level transitions correspond to the bands at the following wavelengths: 250 nm, 272 nm, 338 nm

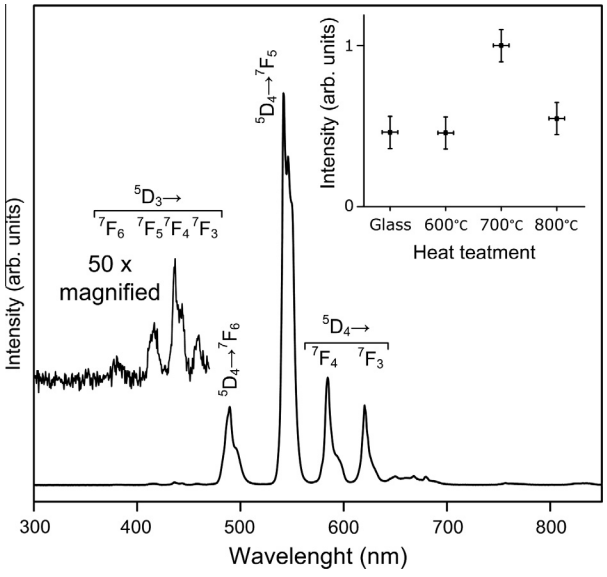

Fig. 4. X-ray induced luminescence spectra of NLF:Tb heat treated at 700 °C; inset shows the dependence of emission intensity on heat-treatment temperature.

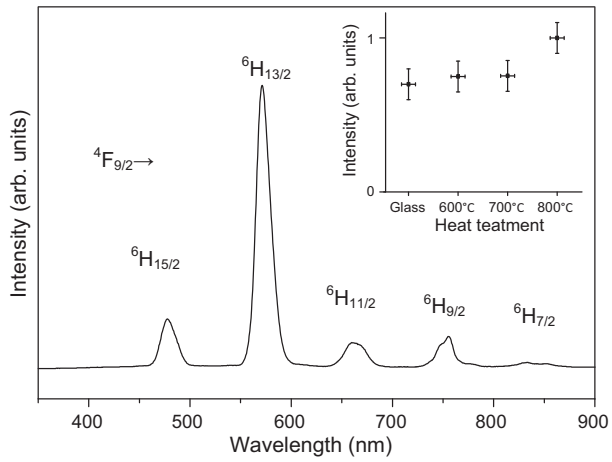

Fig. 5. X-ray induced luminescence spectra of NLF:Dy heat treated at 700 °C; the inset shows the dependence of emission intensity on heat-treatment temperature.

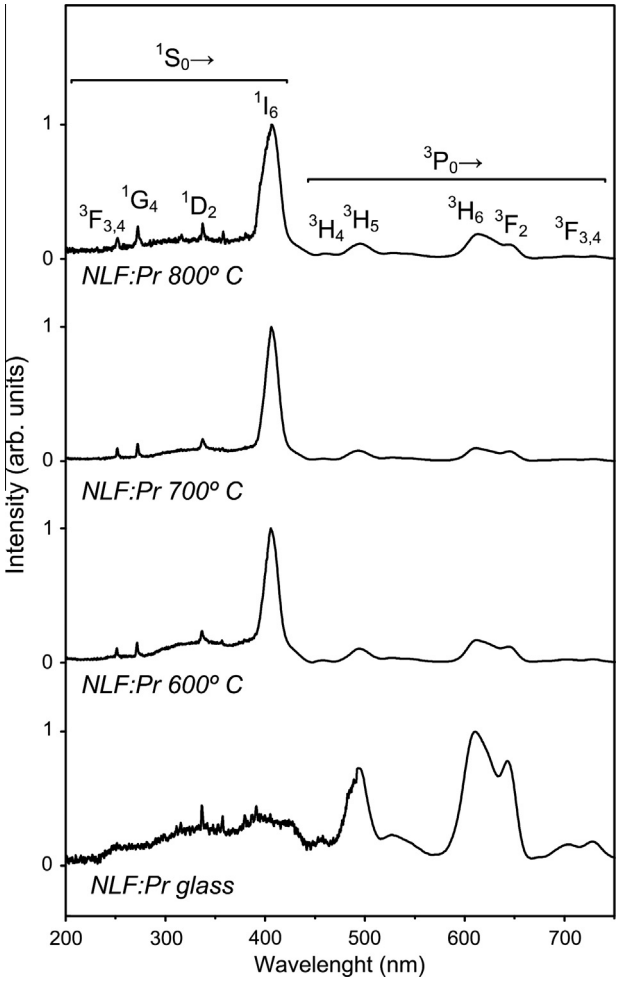

Fig. 6. Normalized X-ray induced luminescence spectra of NLF:Pr heat treated at various temperatures.

and 408 nm. The most intense X-ray induced luminescence peak is located at 408 nm and corresponds to $^1S_0 \rightarrow {}^1I_6$ transition.

The group of energy level transitions $^3P_0 \rightarrow {}^3H_4$, $^3H_5$, $^3H_6$, $^3F_2$ and $^3F_3$ corresponds to the bands at the following wavelengths 492 nm, 532 nm, 609 nm, 643 nm and 686 nm.

The NLF:Pr 700 °C sample has the most intense luminescence.

Spectral shapes of heat treated at various temperatures NLF:Pr are different. Only the heat treated samples have spectral peaks at 408 nm. Therefore, we assume that praseodymium ions could be embedded in a high symmetric environment in glass–ceramics samples.

3.4.4. X-ray induced luminescence of NLF:Nd

The X-ray excited luminescence spectra (Fig. 7) show the intense peak attributed to $^4F_{3/2} \rightarrow {}^4I_{9/2}$ transition at 882 nm. Other peaks are significantly lower. We can observe a group of bands at 275–575 nm. These bands could be attributed to transitions onto the $^4I_{9/2}$ level from the higher energy levels ($^2L_{17/2}$, $^2I_{13/2}$, $^4D_{7/2}$, $^2L_{15/2}$, $^2P_{3/2}$, $^2D_{5/2}$, $^2P_{1/2}$, $^2G_{9/2}$, $^4G_{7/2}$ and $^4G_{9/2}$).

The X-ray excited luminescence spectra also reveal peaks at 620, 823 and 1060 nm attributed to ($^4G_{7/2}$–$^4G_{9/2}$) $\rightarrow {}^4I_{11/2,13/2}$, $^4F_{5/2} \rightarrow {}^4I_{9/2}$, $^4F_{3/2} \rightarrow {}^4I_{11/2}$ transitions, respectively. The NLF:Nd sample heat treated at 800 °C has the most intense luminescence.

The higher luminescence intensities of neodymium ions in glass–ceramics could be explained by the embedding in the corresponding nanocrystals as well.

3.4.5. X-ray induced luminescence: comparison

The NLF:Tb 700 °C sample has also the most intense integrated luminescence among the studied samples. Therefore, we assume intensity of the sample NLF:Tb 700 as 100% to compare X-ray induced luminescence intensities of the samples listed in Table 2. X-ray induced luminescence curve were integrated into the range 350–800 nm for NLF:Tb, NLF:Dy, NLF:Pr samples and 350–1100 nm for NLF:Nd sample because significant peaks are located there.

The samples heat treated at 700 °C or 800 °C have higher intensity of luminescence comparing to the samples with the same dopant treated at lower temperatures.

We also compared the most intense our synthesized sample NLF:Tb 700 °C to well known scintillator CsI:Tl. X-ray induced intensity of NLF:Tb 700 °C is approximately 15% from CsI:Tl intensity (Fig. 8)

3.4.6. Cathodoluminescence spectra

Cathodoluminescence spectra show rare earth electron transition peaks and a wide band extended from about 250 to 500 nm.

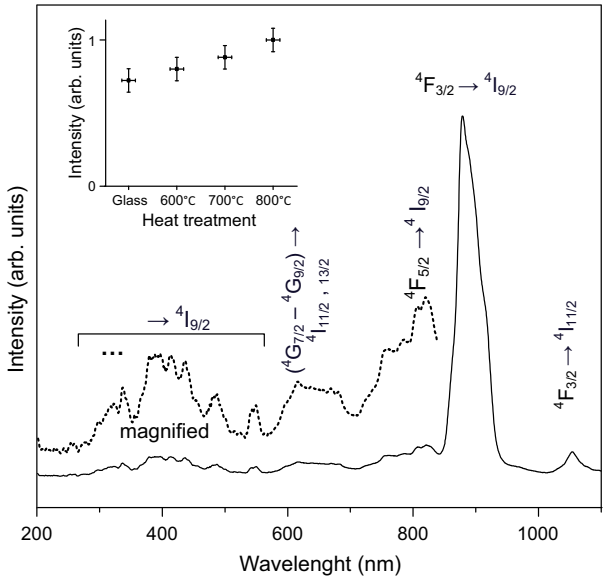

Fig. 7. X-ray induced luminescence spectra of NLF:Nd heat treated at 700 °C; the inset shows the dependence of emission intensity on heat-treatment temperature.

Table 2
Integrated intensity compared with NLF:Tb 700 °C ± 10%.

Sample	Range of integration (nm)	Heat treatment temp.	
		700 °C	800 °C
NLF:Tb	350–800	100%	55%
NLF:Dy	350–800	35%	48%
NLF:Nd	350–800	22%	23%
NLF:Nd	350–1100	43%	50%
NLF:Pr	350–800	26%	22%

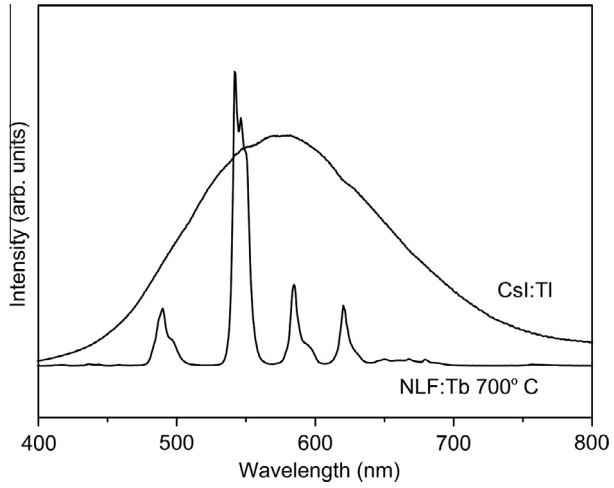

Fig. 8. The intensity of the X-ray induced luminescence of NLF:Tb 700 °C compared to the well known scintillator CsI(Tl) sample of the same size.

The corresponding energy level transitions are indicated in Fig. 9. Spectrum of the nonactivated NLF 700 °C sample shows only a wide band (Fig. 9(e)).

Origin of the wide spectral band of NLF:Dy (Fig. 9(b)), NLF:Pr (Fig. 9(c)), NLF:Nd (Fig. 9(d)) and NLF (Fig. 9(e)) is connected with intrinsic nature of the samples. However, further studies will be necessary before definite conclusions.

We have measured cathodoluminescence decay times for samples heat treated at 700 °C. These results could be approximated by one or two exponents. In case of two exponents we use τ_1 for fast and τ_2 for slow component:

$$f(t) = A_1 \exp(-t/\tau_1) + A_2 \exp(-t/\tau_2) + B, \quad (2)$$

A_i – the decay amplitude, B – constant, τ_i – decay time.

For more convenient comparison of the exponential functions of different samples we have calculated the average exponents of each pair. For this purpose the following formula was used [24]:

$$\langle \tau \rangle = \sum_{i=1}^{2} A_i \tau_i^2 \Big/ \sum_{i=1}^{2} A_i \tau_i. \quad (3)$$

The shortest cathodoluminescence decay times have praseodymium (Fig. 10) and neodymium doped samples heat treated at 700 °C.

Average decay times of the NLF:Tb 700 °C, NLF:Dy 700 °C, NLF:Pr 700 °C and NLF:Nd 700 °C samples measured at maximal cathodoluminescence intensity wavelengths are listed in Table 3.

We must mention that measurements of decay times were available for only in the case of cathodoluminescence. NLF:Nd maximal peak is located outside the spectral range of the CL spectrometer.

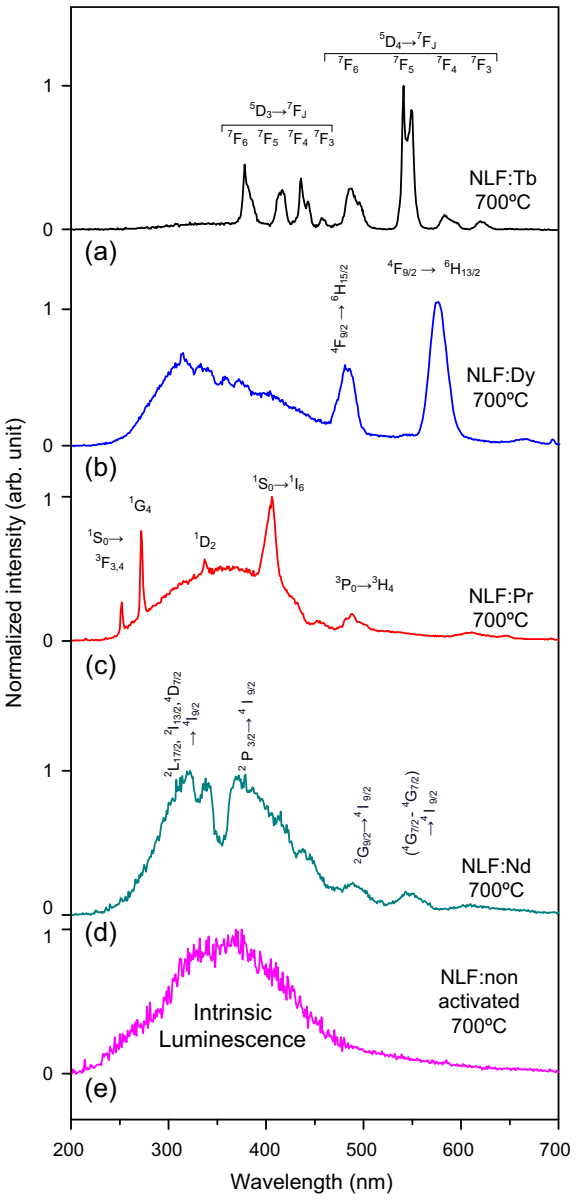

Fig. 9. Normalized cathodoluminescence spectra of NLF:Tb, NLF:Dy, NLF:Pr, NLF:Nd and NLF heat treated at 700 °C.

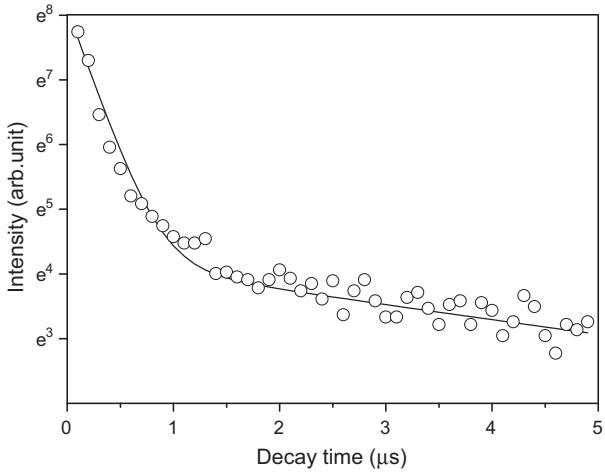

Fig. 10. CL decay curves of NLF:Pr 700 °C measured at 408 nm. Circles represent the experimental data and a solid line represents fitted curves.

Table 3
Average decay times for various samples measured at a maximum of the CL luminescence peak.

Sample	Wavelength (nm)	Transition	Decay time in μs		
			τ_1	τ_2	$\langle\tau\rangle$
NLF:Tb 700 °C	545	$^5D_4 \rightarrow {}^7F_5$	3339	–	3339
NLF:Dy 700 °C	574	$^4F_{9/2} \rightarrow {}^6H_{13/2}$	14	168	152
NLF:Pr 700 °C	408	$^1S_0 \rightarrow {}^1I_6$	0.21	3.93	1.24
NLF:Nd 700 °C	340	$^2L_{15/2}$, $^2I_{13/2}$, $^4D_{7/2} \rightarrow {}^4I_{9/2}$	1.21	3.78	2.75
NLF non doped 700 °C	360	Intrinsic luminescence	1.54	34.56	4.81

4. Conclusions

Terbium, dysprosium, praseodymium and neodymium doped glass–ceramic samples containing $NaLaF_4$ nanocrystals have been produced.

We found out that the presence of crystalline phase enhances the X-ray induced luminescence intensity. According to Scherrer's equation the larger nanocrystals have been formed in the samples subjected to the higher temperature of heat treatment. This trend is observable for heat treatment up to 800 °C.

The average size of $NaLaF_4$ nanocrystals after heat treatment according to Scherrer's equation is from 19 nm to 53 nm.

Scanning electron microscopy of the glass–ceramics shows that a part of rare earth ions could be embedded in $NaLaF_3$ crystallites.

The X-ray induced luminescence of the terbium activated sample treated at 700 °C is the most intense among the studied samples. The praseodymium and neodymium activated samples have fastest cathodoluminescence decay times of 1.24 μs and 2.75 μs, respectively.

The studied samples could be considered for some of scintillator applications. Main peaks of terbium and dysprosium activated samples are located at 545 nm and 574 nm.

Acknowledgements

Financial support from Latvian National Research Program IMIS2 (2014–2017) and ESF Project No. 2013/0046/1DP/1.1.1.2.0/13/APIA/VIAA/021 is gratefully acknowledged. We thank Dr. L. Trinkler and Dr. D. Millers for valuable suggestions and M. Kemere for experimental assistance.

References

[1] M.D. Birowosuto, Novel [gamma]-ray and Thermal-neutron Scintillators: Search for High-light-yield and Fast-response Materials, IOS Press, 2008.
[2] J. Cao, X. Wang, X. Li, Y. Wei, L. Chen, H. Guo, J. Lumin. (2015), http://dx.doi.org/10.1016/j.jlumin.2015.10.049.
[3] G. Blasse, Chem. Mater. 6 (1994) 1465–1475.
[4] T. Kamae, S. Gungi, M. Hirayama, S. Miyazaki, T. Nagato, A. Nakao, H. Murakami, et al., IEEE Trans. 40 (1993) 204–207.
[5] A. de Pablos-Martin, A. Duran, M.J. Pascual, Int. Mater. Rev. 57 (2012) 165–186.
[6] S. Tanabe, H. Hayashi, T. Hanada, N. Onodera, Opt. Mater. 19 (2002) 343–349.
[7] A. Sarakovskis, J. Grube, A. Mishnev, M. Springis, Opt. Mater. 31 (2009) 1517–1524.
[8] G. Doke, A. Sarakovskis, J. Grube, M. Springis, Radiat. Meas. 56 (2013) 27–30.
[9] M.M. Lage, R.L. Moreira, F.M. Matinaga, J.Y. Gesland, Chem. Mater. 17 (2005) 4523–4529.
[10] S. Fujihara, Functionalized Inorganic Fluorides: Synthesis, Characterization and Properties of Nanostructured Solids, vol. 307, 2010, pp. 307–330.
[11] A. de Pablos Martín, G.C. Mather, F. Muñoz, S. Bhattacharyya, Th. Höche, J.R. Jinschek, T. Heil, A. Durán, M.J. Pascual, J. Non-Cryst. Solids 356 (2010) 3071–3079.
[12] A. de Pablos-Martın, S. Soria, M.O. Ramırez, D. Ristic, G.C. Righini, L.E. Bausá, M. J. Pascual, et al., Transparent glass–ceramics: crystallization mechanisms and optical properties, SPIENEWSROOM, 2012. pp. 1–4.
[13] J.P.M. Van der Meer, R.J.M. Konings, D. Sedmidubský, A.C.G. van Genderen, H.A. J. Oonk, J. Chem. Thermodyn. 38 (2006) 1260–1268.
[14] A. Sarakovskis, G. Krieke, G. Doke, J. Grube, L. Grinberga, M. Springis, Opt. Mater. 39 (2015) 90–96.
[15] C.A. Johnson, M. Murayama, K. Küsel, M.F. Hochella, Am. Mineral. 100 (2015) 2091–2105.
[16] W.C. Choy, D. Tao, Solid State Chem. Res. Trends (2007) 23–62.
[17] W.T. Carnall, P.R. Fields, K. Rajnak, J. Chem. Phys. 49 (1968) 4424–4442.
[18] M.R. Babua, N.M. Raoa, A.M. Babua, L. Ramamoorthyb, Int. J. Sci. Res. Publ. 4 (2014) 1–9.
[19] M.A. Gusowski, H.C. Swart, L.S. Karlsson, M. Trzebiatowska-Gusowska, Nanoscale 4 (2012) 541–546.
[20] R. Decadt, K. Van Hecke, D. Depla, K. Leus, D. Weinberger, I. Van Driessche, P. Van Der Voort, R. Van Deun, Inorg. Chem. 51 (2012) 11623–11634.
[21] R. Balda, J. Fernández, E.E. Nyein, U. Hömmerich, Opt. Express 14 (2006) 3993–4004.
[22] A.M. Srivastava, S.J. Duclos, Chem. Phys. Lett. 275 (1997) 453–456.
[23] S. Ismail-Beigi, S.G. Louie, Phys. Rev. Lett. 95 (2005) 156401.
[24] C. Tiseanu, V.A. Lórenz-Fonfría, A. Gessner, M.U. Kumke, B. Gagea, J. Mater. Sci.: Mater. Electron. 20 (2009) 312–316.